

## Analysis of the Spatial Distribution of Seawater Intrusion Using a Hydrogeochemical Approach: A Study of the Coastal Geology of Kebumen Regency, Indonesia

Faidatuz Zahroh, Muhammad Asyroful Mujib\*, Sri Astutik, Bejo Apriyanto, Era Iswara Pangastuti

Department of Geography Education, University of Jember, Jember, 68121, Indonesia

\*Corresponding author, email : [mujib@unej.ac.id](mailto:mujib@unej.ac.id)

### ARTICLE INFO

Received :  
11 September 2022

Revised :  
26 August 2024

Accepted :  
29 August 2024

Published :  
31 August 2024

### ABSTRACT

This study examines seawater intrusion in the southern part of Kebumen District, focusing on the impact of various geological formations on groundwater salinity. Groundwater samples were systematically collected from 11 locations representing alluvial, volcanic, coastal sediment, and karst geological conditions. The samples were analyzed for major ions, including calcium ( $\text{Ca}^{2+}$ ), magnesium ( $\text{Mg}^{2+}$ ), chloride ( $\text{Cl}^-$ ), and bicarbonate ( $\text{HCO}_3^-$ ), as well as Total Dissolved Solids (TDS). Ion ratios such as  $\text{Mg}^{2+}/\text{Ca}^{2+}$ ,  $\text{Cl}^-/\text{HCO}_3^-$ , and  $\text{Mg}^{2+}/(\text{Mg}^{2+}+\text{Ca}^{2+})$ , along with the Fraction of Seawater (fsea), were calculated to assess the extent of seawater intrusion. The study employed the Gibbs diagram method to identify the primary processes controlling groundwater chemistry, revealing that water-rock interactions are dominant in most samples, particularly in those affected by seawater intrusion. The results indicate significant seawater intrusion in alluvial and karst regions, especially at sampling points TP 2, TP 4, and TP 10, while volcanic and coastal sediment areas show minimal intrusion. These findings underscore the critical influence of geological conditions on seawater intrusion and highlight the need for targeted groundwater management strategies. Further research focusing on long-term monitoring is recommended to better understand and mitigate the impacts of seawater intrusion in this region.

**Keywords:** Seawater Intrusion; Groundwater Salinity; Geological Formations; Fraction of Seawater; Ion Ratios

### INTRODUCTION

Seawater intrusion is a widespread environmental problem that affects more than 100 countries worldwide and threatens to degrade the quality and quantity of groundwater in coastal aquifers (Benaafi et al., 2023; Parizi et al., 2019). Coastal areas are situated at a complex and dynamic interface between land and ocean, resulting in the interaction of subsurface movement, both vertical and lateral of seawater with coastal groundwater aquifers (Benaafi et al., 2023; Hussain et al., 2019; Michael et al., 2017). The vulnerability of coastal areas to seawater intrusion is influenced by both natural and anthropogenic factors. Natural factors include global warming (sea level rise and decreased river discharge), tidal effects, storm surges, shoreline erosion, coastal flooding, and the trapping of ancient seawater (Werner et al., 2013; Darmanto & Cahyadi, 2016; Behera et al., 2019; Prusty & Farooq, 2020). Geological factors such as lithology, geomorphology, and structural features also play an important role in controlling seawater

intrusion into aquifers (Prusty & Farooq, 2020). Anthropogenic factors, including agriculture, industry, urban development, and over-pumping of groundwater, have placed coastal groundwater aquifers at risk of seawater intrusion and deterioration (Benaafi et al., 2023; Hussain et al., 2019; Papazotos et al., 2019; Zamroni et al., 2021, 2021).

The risk associated with seawater intrusion in coastal areas is that it may cause the salinity content of groundwater to exceed potable limits, rendering it unusable for human consumption and irrigation (Jasechko et al., 2020; Michael et al., 2017; Werner et al., 2013). The degradation of groundwater quality in coastal areas has become increasingly severe due to human activities. Overexploitation of groundwater, driven by increasing water demand for irrigation, urbanization, industry, fisheries, and electricity, is a significant factor contributing to seawater intrusion in coastal areas (Papazotos et al., 2019; Zamroni et al., 2021).

Techniques used to identify seawater intrusion include geophysical exploration, hydrochemical analysis, isotopic analysis, multivariate statistics, numerical modelling, and simulation techniques (Benaafi et al., 2023; Singhal & Gupta, 2010; Tomaszkievicz et al., 2014; Werner et al., 2013). According to Benaafi et al. (2023), the most widely used techniques for seawater intrusion studies are modelling and simulation techniques (49.4% and 22.3%, respectively), followed by geophysics, hydrochemistry, hydrogeology, and isotope analysis. Prusty & Farooq (2020) broadly divided these methods into direct and indirect methods. Direct methods include the collection and analysis of water samples for physicochemical parameters and isotope analysis, while indirect methods involve the interpretation of bulk resistivity, bulk conductivity, and seismic velocity measurements of aquifer materials, known as geophysical and hydrogeological tests.

Modelling and geophysics have been widely used to identify vulnerabilities to seawater intrusion (Kazakis et al., 2016, 2019; Vann et al., 2020). However, when seawater interacts with freshwater, this interaction alters the chemical composition of the freshwater. Therefore, understanding hydrogeochemical processes is crucial (Nair et al., 2021). Four geochemical processes can change salinity levels in coastal groundwater: (1) freshwater-seawater mixing, (2) carbonate precipitation, (3) ion exchange, and (4) redox reactions (Bear et al., 1999). The most widely utilized hydrogeochemical techniques include ionic ratios of major, minor, and trace elements, ionic deltas, mixing calculations, and geochemical modelling (Shin et al., 2020). A simple and quick indicator for measuring groundwater salinity is the Total Dissolved Solids (TDS) and Electrical Conductivity (EC) parameters (Singhal & Gupta, 2010; Tomaszkievicz et al., 2014). Precise locations for further analysis of major ions such as Na<sup>+</sup>, Cl<sup>-</sup>, Ca<sup>2+</sup>, and Mg<sup>2+</sup>, and minor ions such as Bromide (Br<sup>-</sup>), Fluoride (F<sup>-</sup>), and Iodide (I<sup>-</sup>) have been widely applied (Manivannan & Elango, 2019; Nair et al., 2013; Prusty & Farooq, 2020). Major ions analyzed using ion ratios as leading indicators for seawater intrusion include Na<sup>+</sup>/Cl<sup>-</sup>, HCO<sub>3</sub><sup>-</sup>/Cl<sup>-</sup>, Ca<sup>2+</sup>/Cl<sup>-</sup>, Mg<sup>2+</sup>/Ca<sup>2+</sup>, SO<sub>4</sub><sup>2-</sup>/Cl<sup>-</sup>, Br<sup>-</sup>/Cl<sup>-</sup>, Mg<sup>2+</sup>/(Mg<sup>2+</sup>+Ca<sup>2+</sup>), and Ca<sup>2+</sup>/(HCO<sub>3</sub><sup>-</sup>+SO<sub>4</sub><sup>2-</sup>) (e.g., Kazakis et al., 2016; Kura et al., 2014; Ouhamdouch et al., 2020; Wang et al., 2020; Papazotos et al., 2019; Senthilkumar et al., 2019). The fraction of seawater (f<sub>sea</sub>) is applied to measure freshwater-seawater mixing based on the major anion of freshwater and seawater, chloride (Appelo & Postma, 2005), which has been widely combined with ion ratios in seawater intrusion studies (Abu Al Naeem et al., 2019; Behera et al., 2019; Bourjila et al., 2023; Kumar et al., 2020; Ouhamdouch et al., 2020; Shin et al., 2020; Hasan et al., 2023).

Studies of seawater intrusion in Indonesia using hydrochemical approaches include the coast of Demak Regency, studied through Piper diagram analysis (Darmanto & Cahyadi, 2016; Marfai & Cahyadi, 2017); Parangtritis Beach, with the prediction of the sea-freshwater interface and Base Exchange Index (Wilopo et al., 2021); Wates, Kulon Progo Yogyakarta, with the measurement of groundwater facies through hydrochemical diagrams (Thin et al., 2018); the Semarang City Coast (Ardaneswari et al., 2016); Yogyakarta International Airport, using Piper diagrams and geological conditions (Zamroni et al., 2021); Salt drying ponds in Pademawu Subdistrict, Madura, were studied using physicochemical parameters (Gemilang et al., 2022); similarly, densely populated small islands such as Panggang Island and Pramuka Island in Kepulauan Seribu, Jakarta, were also examined (Cahyadi & Hidayat, 2017).

Aquifer conditions affect the process of seawater intrusion. Previous studies of seawater intrusion have primarily focused on alluvial plains (Ardaneswari et al., 2016; Bourjila et al., 2023; Marfai & Cahyadi, 2017; Radityo et al., 2020) and karst or limestone areas (Cahyadi et al., 2017; Cahyadi & Hidayat, 2017; Tomaszkiwicz et al., 2014). The high porosity of karst facilitates seawater intrusion (Yang et al., 2022). Different aquifer conditions impact the intrusion process. This research is of particular interest because the study area features two natural landscapes: the South Gombong Karst landscape and alluvial plains. Hindarto & Ansori (2021) found that the South Gombong Karst landscape has significant potential, such as for geotourism and natural resources like minerals and water. Mujib et al. (2020) stated that springs in karst landscapes are crucial for consumption, irrigation, industry, and other domestic needs. However, water in karst areas is vulnerable to contamination, including seawater intrusion.

The research site presents an interesting study area, as previous field conditions and research have indicated that seawater could be detected up to 5 km inland. Seawater intrusion, which infiltrates land areas to varying distances, depends on the level of intrusion. For instance, at Ketah Beach in Situbondo, the intrusion reaches up to 1 km (Putri et al., 2016); at Barombong, Makassar, it extends to 1.5 km (Yanti et al., 2016); and the furthest distance observed was 4 km along the coast of Tegal City (Ismawan et al., 2016). Due to the limited sampling from several groundwater wells representing the geological conditions in the study area, the spatial distribution of data points such as groundwater and soil was interpolated using geostatistical analysis. This study mapped ion ratios and the fraction of seawater using IDW (Inverse Distance Weighting) analysis, a method widely applied with weight variations ranging from 1 to 3 (Arslan, 2014; Kura et al., 2014; Momejian et al., 2019). The objective of this study was to spatially map seawater intrusion based on a hydrogeochemical approach across four coastal geological conditions: alluvial, coastal sediment, volcanic, and karst.

## METHODS

### Study Area

The research location is in the southern part of Kebumen District, characterized by a sloping plain to hilly topography. The geological formations in the study area, from oldest to youngest, include the Gabon Formation (Early Miocene), Andesite (Early Miocene to Middle Miocene), Kalipucang Formation (Middle Miocene), Halang Formation (Late Miocene), and Quaternary Alluvium and Coastal Deposits (Figure 1). The Gabon Formation consists of breccia with andesite components, a basic tuff matrix, coarse sandstone, local lapilli tuff, lava, and lahar deposits, which are generally altered (Asikin et al., 1992). This formation exhibits proximal facies characteristics of volcanoes. Within the Gabon Formation, there are occurrences of andesite in the form of partial dikes. Andesite is characteristic of the central and proximal facies of each Tertiary volcano in the southern mountains of Central Java, including the Kulon Progo Mountains (Zamroni et al., 2021). The Kalipucang Formation is composed of reef limestone, locally clastic limestone, and bituminous shale at the base. The younger sedimentary rock is the Halang Formation, which consists of interbedded sandstone, claystone, marl, and tuff with breccia inserts, influenced by turbidity currents and underwater sliding (Asikin et al., 1992). The Kalipucang Formation is part of the Gombong Karst area, which has a karstification development (Dk) level of Dk=8, similar to the Gunungsewu Karst area (Mujib et al., 2024). The eastern part of the study area is dominated by Quaternary Alluvium, consisting of alluvial deposits distributed along river basins and near coastal areas. Alluvium sediments are composed of clay, silt, sand, and gravel, while beach sediments near the coast consist of well-sorted sand with a very loose grain structure.

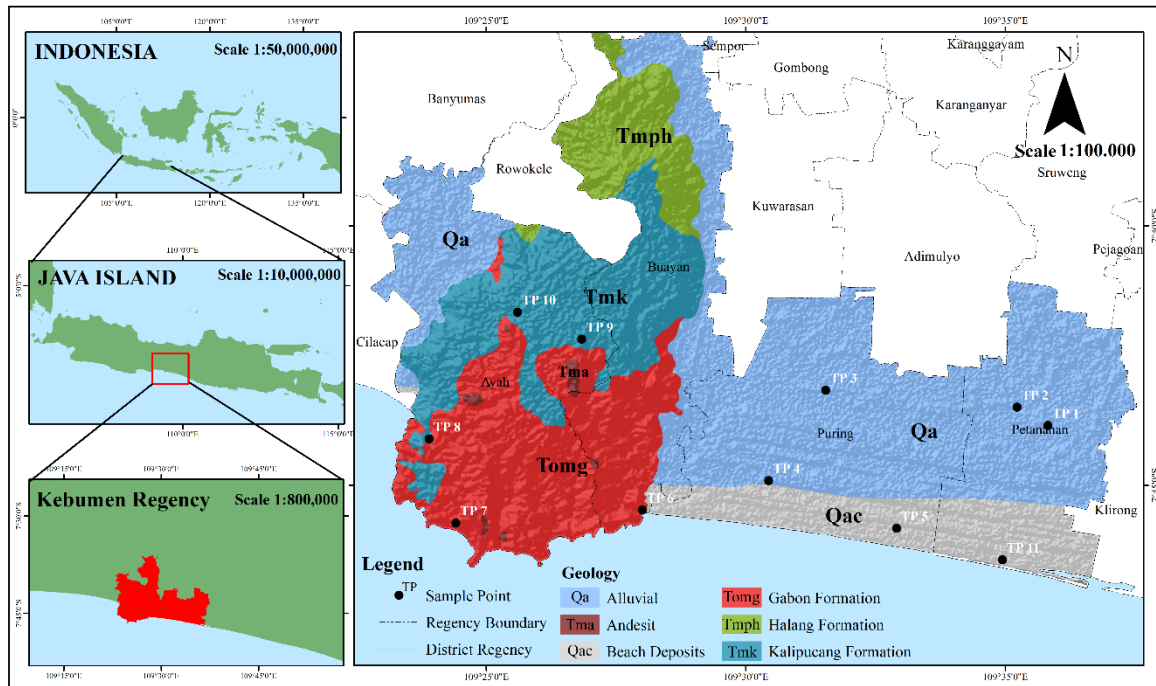


Figure 1. Geological map and groundwater sampling point

### Materials and Data Collection

The materials used in this study consisted of water samples collected for the analysis of physical and chemical quality. Specifically, 11 samples were taken for Total Dissolved Solids (TDS) measurements, and 11 samples were analyzed for major ions, including calcium ( $\text{Ca}^{2+}$ ), magnesium ( $\text{Mg}^{2+}$ ), chloride ( $\text{Cl}^-$ ), and bicarbonate ( $\text{HCO}_3^-$ ). Standard methods were employed for these analyses, adhering to SNI 06-6989 and APHA 2017 guidelines. Additionally, the chloride content in 11 samples was determined using the titration method with mercuric nitrate, utilizing the Chloride Test Kit HI 3815. The accuracy of ion measurements was verified using Charge Balancing Error (CBE) analysis (Equation 1). The CBE calculation required converting the major ion units from milligrams per liter to milliequivalents per liter.

$$CBE(\%) = \frac{\sum cation - \sum anion}{\sum cation + \sum anion} \times 100 \quad (\text{Eq.1})$$

The sample preparation involved systematic collection and preservation procedures to ensure the integrity of the water quality data. Each of the 11 water samples was collected in pre-cleaned polyethylene bottles to prevent contamination. The samples were filtered using 0.45  $\mu\text{m}$  pore size membrane filters to remove particulate matter before chemical analysis. For TDS measurements, the samples were dried at 180°C to ensure consistent weight. In the analysis of major ions, the samples were treated with appropriate reagents to ensure the accurate detection of  $\text{Ca}^{2+}$ ,  $\text{Mg}^{2+}$ ,  $\text{Cl}^-$ , and  $\text{HCO}_3^-$  ions, following SNI 06-6989 and APHA 2017 standards. Chloride samples were specifically prepared using the Chloride Test Kit HI 3815 to ensure precise titration analyses.

### Data Analysis

The experimental setup was meticulously designed to measure various water quality parameters. The TDS classification was performed by categorizing the samples into five distinct classes: Fresh groundwater (0-500 mg/L), Slightly saline groundwater (500-1500 mg/L), Moderately saline groundwater (1500-7000 mg/L), Highly saline groundwater (7000-15000 mg/L), and Seawater (>35000 mg/L). The ion ratio parameter was also used to classify water

salinity. In this study, three ion ratios were employed:  $Mg^{2+}/Ca^{2+}$ ,  $Cl^-/HCO_3^-$ , and  $Mg^{2+}/(Mg^{2+}+Ca^{2+})$ . The criteria for assessing the impact of seawater intrusion using ion ratios are outlined in Table 1.

Table 1. Ion Ratio Criteria for Determining the Effect of Intrusion

Ratio Ions	Value	Criteria
$Mg^{2+}/Ca^{2+}$	>1	Affected by seawater intrusion
	<1	Not affected by seawater intrusion
$Cl^-/HCO_3^-$	<0.5	Not affected by seawater intrusion
	0.5-1.3	Slightly affected by seawater intrusion
	1.3-2.8	Moderately affected by seawater intrusion
	2.8-6.6	Severely affected by seawater intrusion
	>6.6	Very severely affected by seawater intrusion
$Mg^{2+}/(Mg^{2+}+Ca^{2+})$	>0.5	Affected by seawater intrusion
	<0.5	Not affected by seawater intrusion

**Note :** Adapted from Kura et al. (2014), Kazakis et al. (2016), Behera et al. (2019), Shin et al. (2020), Kumar et al. (2020), Wang et al. (2020), Ouhamdouch et al. (2021).

The primary factors controlling the chemical interaction processes in groundwater within the aquifer at the study site are illustrated using a Gibbs diagram. There are three general processes that govern these chemical interactions: evaporation-crystallization, water-rock interaction, and precipitation dominance, which are depicted in two scatter plots. Due to the limited data available for the Na parameter in this study, a scatter plot with the x-axis representing the molar ratio  $Cl^-/(Cl^-+HCO_3^-)$  and the y-axis representing the logarithmic scale of TDS was used. In aquifers where chemical interactions are dominated by evaporation, the values of  $Na^+$ ,  $Cl^-$ , and TDS are high, while aquifers dominated by water-rock interaction exhibit high values of  $Ca^{2+}$  and  $HCO_3^-$  (Yang et al., 2022).

Additionally, the Fraction of Seawater ( $f_{sea}$ ) is a parameter used to identify seawater intrusion by measuring the chloride concentration (meq/L) in both freshwater and seawater. The freshwater chloride concentration selected from the study location is the average chloride value for water with an electrical conductivity (EC) below 1000  $\mu S/cm$ , while the seawater chloride concentration is obtained from laboratory tests. The mixing level of seawater and freshwater in this equation is defined on a scale from 0 to 100. A lower  $f_{sea}$  value indicates fresher groundwater at the study site. The Fraction of Seawater ( $f_{sea}$ ) was determined using Equation 2.

$$f_{sea} = \frac{Cl_{sample} - Cl_{freshwater}}{Cl_{seawater} - Cl_{freshwater}} \quad (Eq.2)$$

where  $Cl_{sample}$  represents the chloride concentration in the sample,  $Cl_{freshwater}$  is the average chloride concentration in freshwater samples with electrical conductivity (EC) below 1 dS/m, and  $Cl_{seawater}$  is the chloride concentration in seawater obtained from laboratory tests. This ratio facilitated the identification of seawater intrusion in the study area.

The spatial distribution of seawater intrusion was mapped using interpolation methods between study points based on the  $Mg^{2+}/Ca^{2+}$ ,  $Cl^-/HCO_3^-$ ,  $Mg/(Mg+Ca)$ , and  $f_{sea}$  ratios. ArcGIS 10.8 software with the IDW (Inverse Distance Weighting) method was employed for this purpose, following the methodologies of Tomaszewicz et al. (2014) and Hadi (2013) to ensure accurate spatial representation.

## RESULTS AND DISCUSSION

### Hydrogeochemical Characteristics

The physicochemical parameters and major ion compositions in the study area are presented in Table 2 and illustrated in Figure 3. The dominant cations analyzed were  $\text{Ca}^{2+}$  and  $\text{Mg}^{2+}$ , while the dominant anions were  $\text{Cl}^-$  and  $\text{HCO}_3^-$ .  $\text{Mg}^{2+}$  concentrations ranged from 3.87 to 59 mg/L, with an average of 16.71 mg/L (c.v. = 89.1%). The highest  $\text{Mg}^{2+}$  level of 59 mg/L was recorded at TP 2 in Desa Karangduwur, characterized by alluvial geology, whereas the lowest value of 3.87 mg/L was found at TP 5 in Desa Sidoharjo, with beach sediment geology. High Mg levels can be influenced by seawater intrusion (Wang et al., 2020).

The second most dominant cation was  $\text{Ca}^{2+}$ , with values ranging from 12.74 to 133.73 mg/L and an average of 44.73 mg/L (c.v. = 74.13%). The highest  $\text{Ca}^{2+}$  concentration of 133.73 mg/L was recorded in the alluvial geological setting at TP 2. The dominant anion in the groundwater samples was  $\text{Cl}^-$ , with concentrations ranging from 10.9 to 496.3 mg/L and an average of 85.9 mg/L (c.v. = 166.20%). The highest  $\text{Cl}^-$  concentration of 496.3 mg/L was also found at TP 2, suggesting a significant influence of seawater intrusion.

Table 2. Chemical composition of groundwater samples

Sample ID	Location	Geology	Temp °C	pH	TDS ppm	Mg mg/l	Ca mg/l	Cl mg/l	HCO <sub>3</sub> mg/l
TP 1	Kebonsari, Petanahan	Alluvial	24.2	6.9	367	12.57	28.66	55.1	465
TP 2	Karangduwur, Petanahan	Alluvial	24.2	6.9	977	59	133.73	496.3	585.8
TP 3	Sitiadi, Puring	Alluvial	24.2	7.2	450	22.73	48.56	99.3	175.1
TP 4	Surorejan, Puring	Alluvial	24.2	8	666	14.51	12.74	148.9	175.1
TP 5	Sidoharjo, Puring	Beach Sediment	24.2	7.3	145	3.87	30.25	15.4	96.6
TP 6	Karangbolong, Buayan	Volcanic (Gabon)	24.2	7	149	12.57	25.47	35.2	114.7
TP 7	Karangduwur, Ayah	Volcanic (Gabon)	24.2	6.9	199	12.57	60.6	33.7	205.3
TP 8	Argopeni, Ayah	Volcanic (Gabon)	24.2	7.3	149	11.12	38.21	20.8	96.6
TP 9	Watukelir, Ayah	Karst (Kalipucang)	24.2	7.2	259	9.19	60.5	12.4	199.3
TP 10	Tlogosari, Ayah	Karst (Kalipucang)	24.2	7.1	143	17.89	27.86	10.9	60.4
TP 11	Karanggadung, Petanahan	Beach Sediment	24.2	7.1	96	774	25.47	16.9	223.4
	min		24.2	6.9	96	3.87	12.74	10.9	60.4
	max		24.2	8	977	59	133.73	496.3	585.8
	mean		24.2	7.17	327.27	16.71	44.73	85.90	217.94
	$\sigma$		-	0.31	275.48	14.88	33.16	142.76	162.94
	c.v (%)		-	4.37	84.17	89.10	74.13	166.20	74.76

Note:  $\sigma$  standard deviation; c.v Coefficient of Variation  $[(\sigma/\text{mean})\times 100]$

$\text{HCO}_3^-$  levels varied widely, with the highest concentration of 585.8 mg/L observed in the alluvial geological area at TP 2. The high  $\text{HCO}_3^-$  concentration indicates carbon dioxide dissolution in water, which is enhanced by the ionization of carbonic acid (Renaldo, 2019). Notably, the alluvial geological areas exhibited the highest variability in TDS,  $\text{Cl}^-$ , and  $\text{HCO}_3^-$  parameters, suggesting complex hydrogeochemical processes. The highest standard deviations were observed for TDS in the alluvial samples, highlighting significant spatial variability in these regions. Variations in the physical and chemical parameters of groundwater in four coastal geological conditions are shown in the boxplot diagram (Figure 2).

The highest  $Mg^{2+}$  concentration in the alluvial geological area at TP 2 is attributed to the dissolution of ferrous magnesium and magnesium carbonate from rocks, as well as the significant influence of seawater (Renaldo, 2019). The alluvial geology, characterized by permeable sediments, facilitates the mixing of groundwater with seawater, thereby increasing the  $Mg^{2+}$  content. Similarly, the high  $Ca^{2+}$  concentration at TP 2 can be linked to seawater intrusion and the dissolution of calcite and other carbonate minerals (Renaldo, 2019). Freshwaters typically exhibit  $Ca^{2+}$  concentrations around 15 mg/L, while waters near carbonate rocks and marine environments range from 30 to 400 mg/L (Renaldo, 2019). The observed values at TP 2 exceed these ranges, indicating substantial seawater mixing.

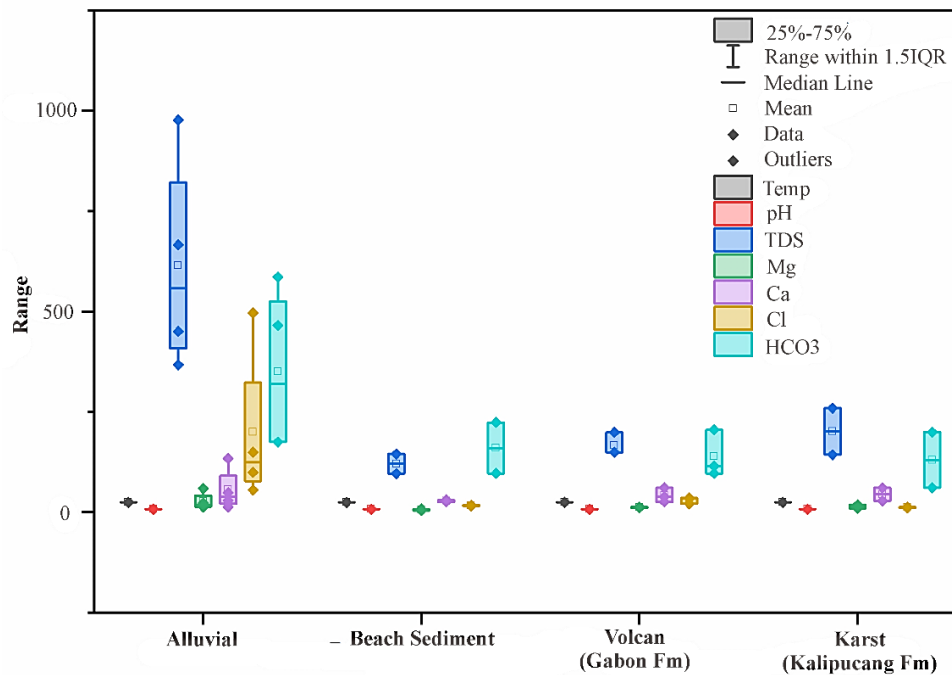


Figure 2. Boxplot diagram of physicochemical properties of groundwater

The elevated  $Cl^-$  concentrations at TP 2 further support the hypothesis of seawater intrusion, as  $Cl^-$  is a major ion in seawater with concentrations around 19,300 mg/L (Panjaitan et al., 2018). The  $Cl^-/HCO_3^-$  ratio at TP 2 suggests significant seawater influence, corroborated by high  $Cl^-$  values exceeding typical freshwater ranges of 2-20 mg/L (Renaldo, 2019). This finding is critical as it highlights the potential for seawater intrusion to alter groundwater chemistry in coastal alluvial areas, impacting water quality and availability.

The highest  $HCO_3^-$  concentration recorded in the alluvial geological area at TP 2 indicates significant carbon dioxide dissolution and subsequent bicarbonate formation. Bicarbonate levels in freshwater typically remain below 500 mg/L at a pH of 7-8, but the concentration at TP 2 exceeded this threshold, suggesting enhanced carbonic acid ionization (Mujib, 2015; Sunardi, 2006). The elevated bicarbonate levels in the TP 2 sample align with the findings of Renaldo (2019), who noted that ionization processes can significantly increase bicarbonate concentrations in groundwater. The presence of seawater intrusion, indicated by the  $Cl^-/HCO_3^-$  ratio, further substantiates the impact of seawater on the hydrogeochemical characteristics of the area.

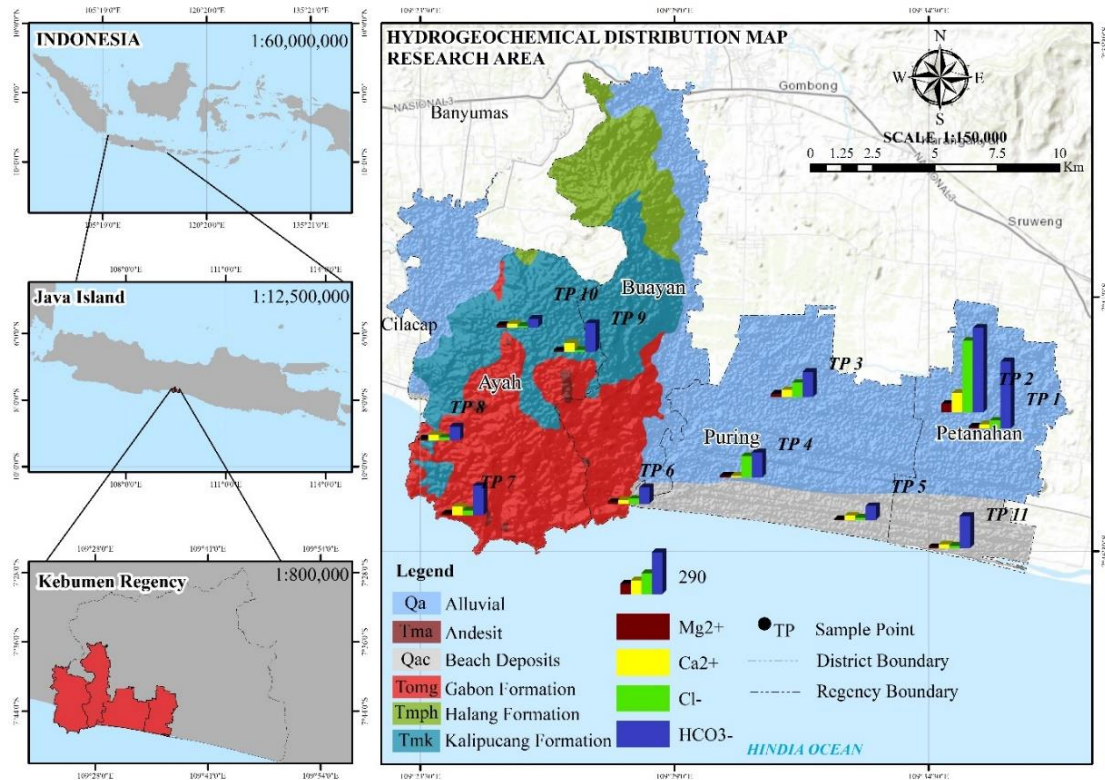


Figure 3. Hydrogeochemical Distribution Map of the Research Area

### Classification of Total Dissolved Solids (TDS)

Table 3 categorizes the Total Dissolved Solids (TDS) levels in the study area into five classes, with the majority falling into Class 1 (Fresh groundwater) and Class 2 (Slightly saline groundwater). Specifically, 81.8% (9 samples) of the samples are classified as fresh groundwater, observed in geological settings such as alluvial, volcanic, beach sediment, and karst. These samples are located 0.1 to 8 kilometers from the coastline. The remaining 18.2% (2 samples), identified as slightly saline groundwater, include TP 2 and TP 4, both situated in alluvial geological settings. TP 2 is 6.4 kilometers from the coastline, and TP 4 is approximately 2.2 kilometers away. The spatial distribution of seawater intrusion based on TDS is shown in Figure 4a.

Table 3. Classification of Total Dissolved Solids (TDS) based on seawater intrusion

Class	TDS (mg/L)	Number of Samples	%	Sample Locations
Fresh groundwater	0-500	9	81.8	TP 1, 3, 5, 6, 7, 8, 9, 10, 11
Slightly saline groundwater	500-1500	2	18.2	TP 2 and TP 4
Moderately saline groundwater	1500-7000	0	0.0	
Highly saline groundwater	7000-15000	0	0.0	
Very Highly saline groundwater	15000-35000	0	0.0	
Seawater	>35000	0	0.0	

The findings from the TDS classification align with established research on groundwater salinity levels in coastal regions. Similar to the findings of Setiawan (2014), the presence of fresh groundwater in various geological conditions and distances from the coastline underscores the diverse impact of geological formations on groundwater quality. The study by Cahyadi et al. (2017) on the spatial distribution of water salinity on Pramuka Island further supports these

observations, highlighting the influence of aquifer formation processes and the depositional environment on ion concentrations.

### Ion Ratios

The analysis of ion ratios presented in Table 4 provided a detailed understanding of seawater intrusion across various geological formations. In the Alluvial geological area, TP 4 exhibited the highest  $Mg^{2+}/Ca^{2+}$  ratio at 1.88 meq/l, indicating affected by seawater intrusion. Similarly, TP 10 in the Karst geological area also showed a notable  $Mg^{2+}/Ca^{2+}$  ratio of 1.06 meq/l, suggesting intrusion. The  $Cl^-/HCO_3^-$  ratios further highlighted the presence of seawater intrusion, particularly at TP 2, TP 3, TP 4, and TP 6 where the ratios were 1.46, 0.96, 1.46, and 0.53 meq/l, respectively, classifying these locations as slightly and moderately affected by seawater intrusion. The  $Mg^{2+}/(Mg^{2+}+Ca^{2+})$  ratio also indicates the same locations as the  $Mg^{2+}/Ca^{2+}$  ratio, specifically TP 4 and TP 10, which are impacted by seawater intrusion, with values of 0.65 and 0.61 meq/l, respectively.

Table 4. Ion Ratios [ $Mg/Ca$ ,  $Cl/HCO_3$ , and  $Mg/(Mg+Ca)$ ]

Geology	Sample ID	Ion Ratios			Distance to beach meter
		$Mg/Ca$ meq/l	$Cl/HCO_3$ meq/l	$Mg/(Mg+Ca)$ meq/l	
Alluvial	TP 1	0.72	0.20	0.42	5600
	TP 2	0.73	1.46 (c)	0.42	6400
	TP 3	0.77	0.98 (b)	0.44	5500
	TP 4	1.88 (a)	1.46 (c)	0.65 (a)	2200
Volcan	TP 6	0.81	0.53 (b)	0.45	100
	TP 7	0.34	0.28	0.25	300
	TP 8	0.48	0.37	0.32	200
Karst	TP 9	0.25	0.11	0.20	7600
	TP 10	1.06 (a)	0.31	0.51 (a)	8100
Beach Sediment	TP 5	0.21	0.27	0.17	300
	TP 11	0.50	0.13	0.33	100

**Note:**  $Mg/Ca$  and  $Mg/(Mg+Ca)$  : (a)affected by seawater intrusion

$Cl/HCO_3$  : (b)Slightly affected by seawater intrusion; (c)Moderately affected by seawater intrusion

The findings from Table 4 align with Kura et al. (2014), Kazakis et al. (2016), Abu Al Naem et al. (2019), and Kumar et al. (2020), who emphasized the relevance of  $Mg^{2+}/Ca^{2+}$ ,  $Cl^-/HCO_3^-$ , and  $Mg^{2+}/(Mg^{2+}+Ca^{2+})$  ratios in detecting seawater intrusion. The slightly and moderately affected by seawater intrusion of TP 2, TP 3, TP 4, and TP 6, despite varying distances from the coast, suggests that geological formations significantly influence the degree of intrusion. For instance, TP 6, located merely 100 meters from the coast, exhibits a lower ion ratio compared to TP 4, which is 2.2 km inland. This highlights the complex interaction between distance, geology, and seawater intrusion.

The significant intrusion observed at TP 2, TP 4 and TP 10 across different geological settings underlines the susceptibility of alluvial and karst formations to seawater encroachment. The comparative analysis of ion ratios reveals that TP 2, TP 4 and TP 10 are the most affected by seawater intrusion. The intrusion at TP 2 and TP 4 in the alluvial geological area is particularly significant, as indicated by the highest  $Mg/Ca$  ratio of 1.88 meq/l and  $Cl^-/HCO_3^-$  ratio of 1.46 meq/l at TP 4. The ion ratio values in the coastal sediments, particularly at TP 5 and TP 11, show much lower values, indicating minimal intrusion despite their proximity to the shoreline.

Groundwater affected by seawater intrusion, based on the  $Mg^{2+}/Ca^{2+}$  ion ratio, has a value above the mixing ratio of 1. The  $Mg^{2+}/(Mg^{2+}+Ca^{2+})$  ratio is above 0.5 at TP 4 and TP 10, indicating seawater intrusion (Figures 4a and 4c). The relationship between  $Ca^{2+}$ ,  $Mg^{2+}$ , and  $Cl^-$  is depicted

to illustrate the ion characteristics of salinity. At TP 4 and TP 10, both ion ratios indicate an increase in  $Mg^{2+}$  during the groundwater ion exchange process, serving as an indicator of intrusion, while  $Ca^{2+}$  shows a lower concentration (Kumar et al., 2020; Wang et al., 2020). In  $Cl^-/HCO_3^-$ , the mixing ratio values are 0.5 and 1.3, observed at TP 2, TP 3, TP 4, and TP 6 (Figure 4b).  $Cl^-$  ions are abundant in saline water, making them an indicator of intrusion in fresh groundwater. The relationship between  $Cl^-/HCO_3^-$  and  $Mg^{2+}/Ca^{2+}$  is shown in Figure 4d. Samples based on these two ion ratios exhibit slight variations, indicating groundwater geochemical processes such as cation exchange (Kumar et al., 2020). The spatial distributions of the three ion ratios are presented in Figures 5b, 5c, and 5d.

The findings from this study are consistent with those of Tomaszekiewicz et al. (2014), who highlighted the importance of geological and hydrological factors in controlling groundwater salinity. The variation in ion ratios across different formations demonstrates the complex interplay of these factors in influencing seawater intrusion. The higher intrusion observed in the Kalipucang Formation, as reflected in the  $Mg^{2+}/Ca^{2+}$  and  $Cl^-/HCO_3^-$  ratios, can be attributed to the lithological composition of limestone, which is prone to chemical processes that enhance salinity.

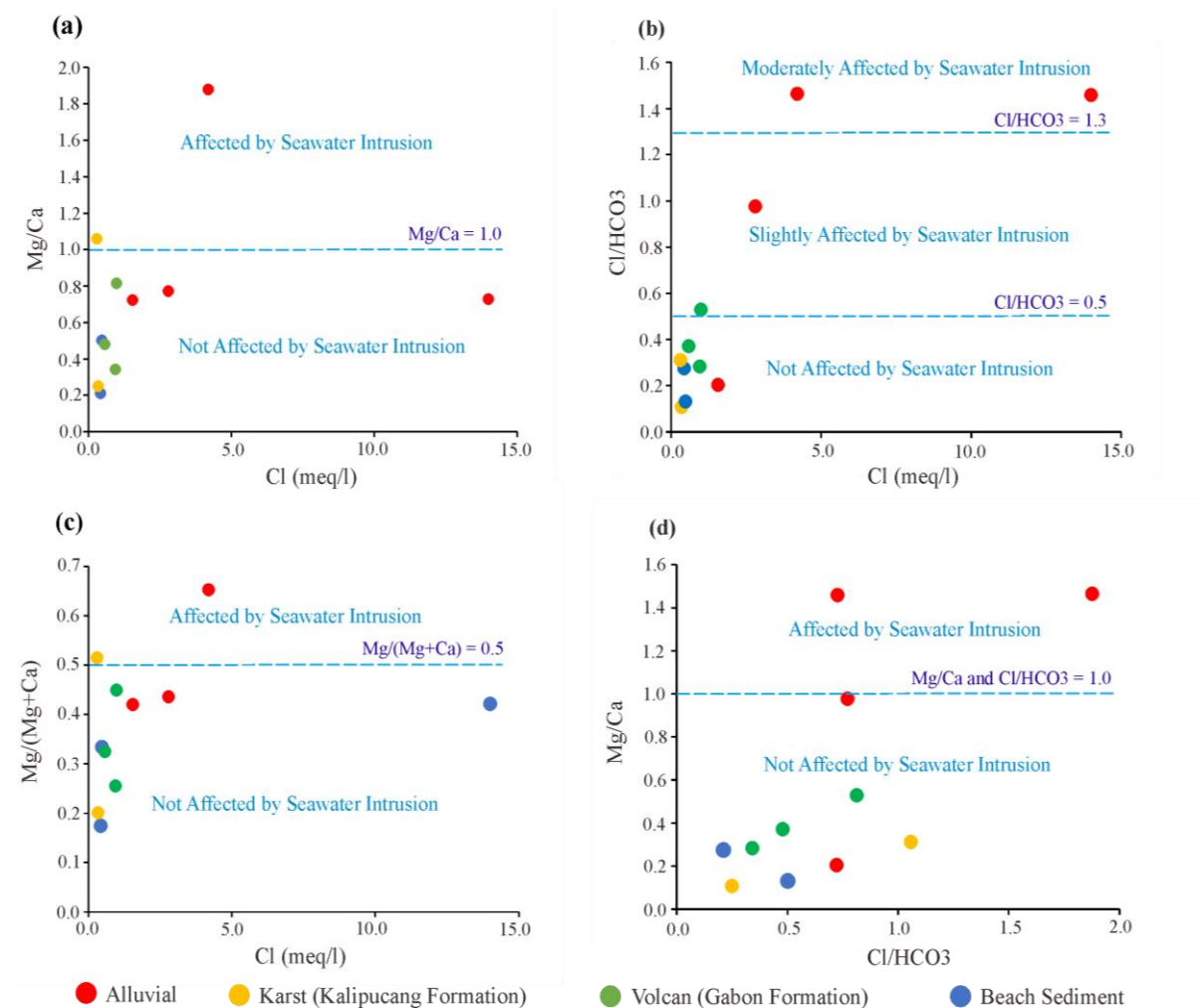


Figure 4. Ion ratio to show samples affected by seawater intrusion (a) Cl vs. Mg/Ca; (b) Cl vs. Cl/HCO<sub>3</sub>; (c) Cl vs. Mg/(Mg+Ca); and (d) Mg/Ca vs Cl/HCO<sub>3</sub>.

The implications of these findings are critical for coastal water resource management. The identification of high intrusion areas, such as TP 2, TP 4 and TP 10, provides essential information for developing targeted strategies to mitigate the effects of seawater intrusion. Understanding

the specific geological conditions that contribute to higher intrusion levels allows for more effective monitoring and management practices, particularly in vulnerable formations like the Kalipucang and alluvial areas. This study underscores the need for continued research and monitoring to protect freshwater aquifers from salinization.

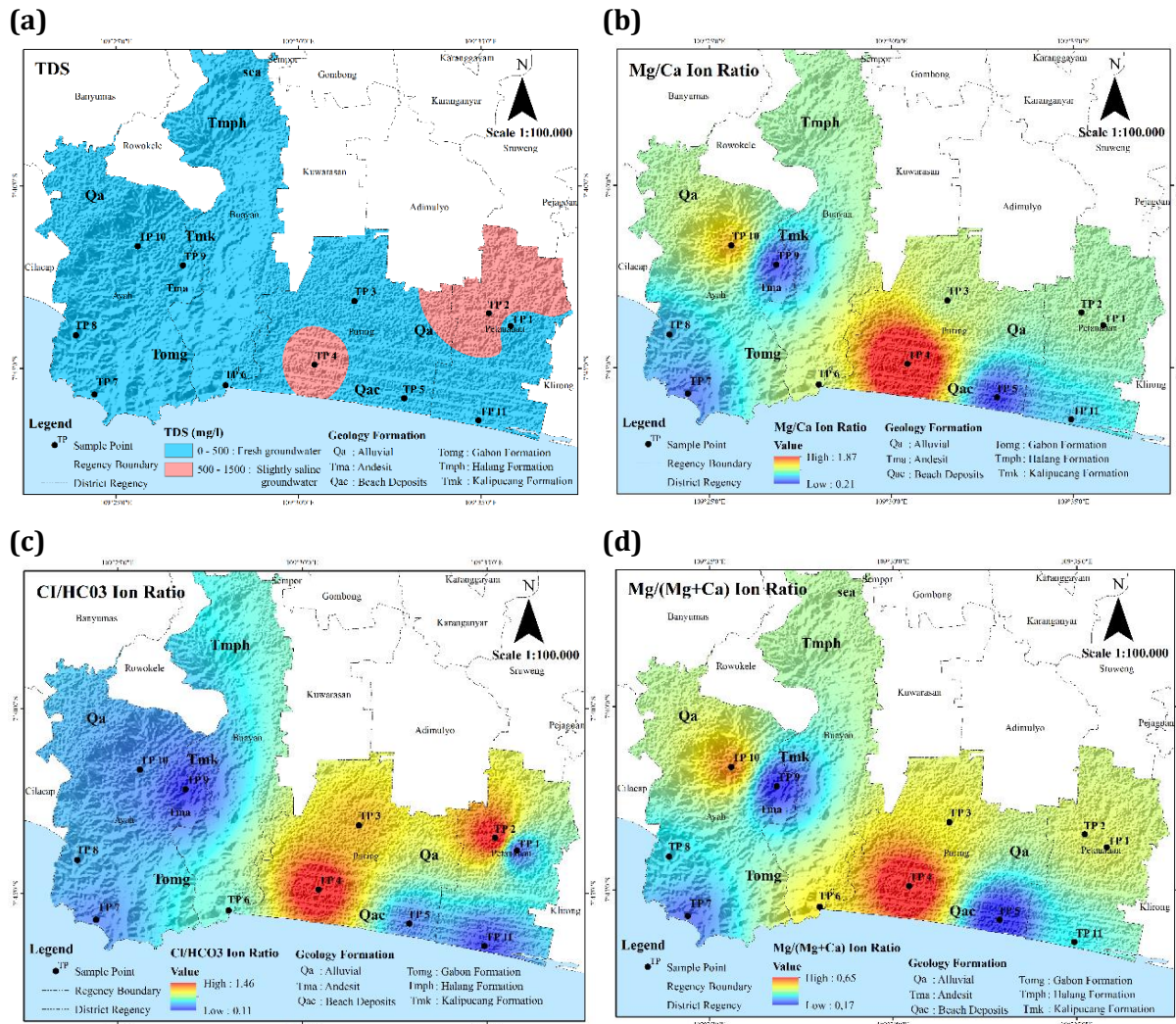


Figure 5. Distribution of TDS and ion ratios: (a) Classification of TDS based on seawater intrusion; (b) Mg/Ca ion ratio; (c) Cl/HCO<sub>3</sub> ion ratio; and (d) Mg/(Mg+Ca) ion ratio

### Mechanisms Controlling Groundwater Chemistry

The Gibbs diagram in Figure 6 provides a clear visual representation of the dominant processes controlling groundwater chemistry in the study area. Most of the groundwater samples, including those from TP 2 and TP 4, fall within the region dominated by rock-water interaction, indicating that this process was the primary control on the geochemical composition of the groundwater, with minerals in the rock dissolving into the water and serving as the primary source of ions (Razi et al., 2024; Wang et al., 2020). The moderate TDS values observed in these samples, combined with their positioning in the diagram, suggest that the interaction between the groundwater and the surrounding geological formations was the key factor in determining the water chemistry.

The data from the Gibbs diagram align with previous research, including Wang et al. (2020) and Razi et al. (2024), which indicated that water-rock interaction was a significant process in the geochemical evolution of groundwater, particularly in areas with moderate

salinity. In this study, even the samples affected by seawater intrusion, such as TP 2 and TP 4, showed a strong influence of water-rock interaction, as opposed to evaporation-crystallization processes. This was evident from their lower TDS values and their position within the central region of the diagram, which was indicative of moderate salinity and a dominance of rock-water interactions.

The dominance of rock-water interaction in controlling groundwater chemistry in the study area had important implications for understanding the geochemical processes at play. The presence of Ca and HCO<sub>3</sub> in the water, as suggested by the position of the samples in the Gibbs diagram, highlighted the dissolution of carbonate minerals from the surrounding rock formations. This process not only contributed to the overall ion concentration in the water but also influenced the buffering capacity of the groundwater, making it less susceptible to pH changes and other external influences.

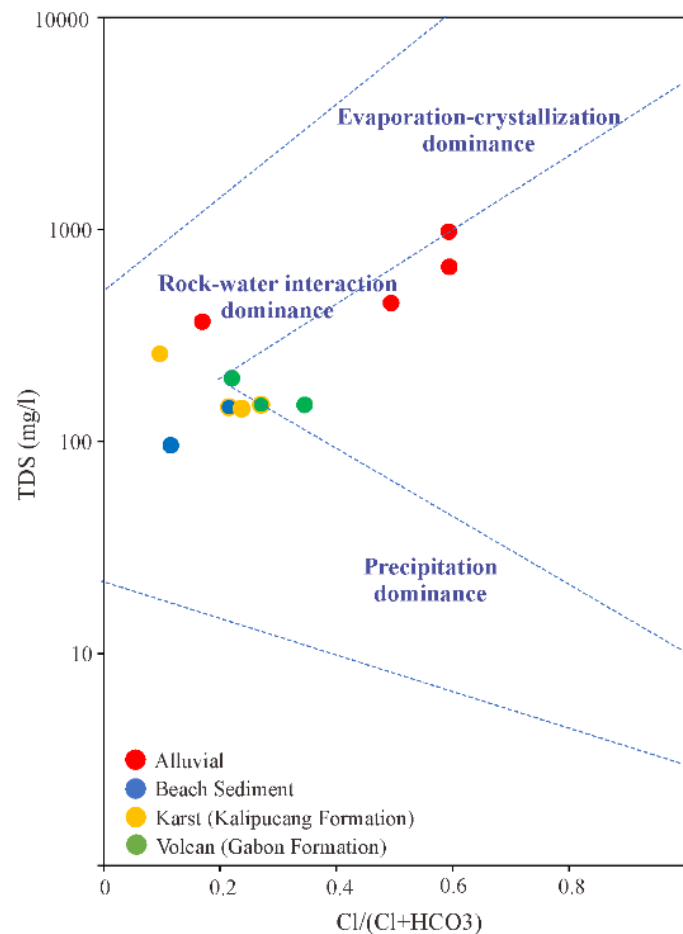


Figure 6. Gibbs diagram showing the dominant processes controlling groundwater chemistry in the study area

### The Fraction of Seawater ( $f_{sea}$ )

The results of calculating the fraction of seawater based on the chloride concentration in 11 research samples are summarized in Table 2. The average chloride concentration for fresh water was 2.42 meq/l, calculated from the average chloride values at research sites with a DHL value <1000 mS/cm. The seawater chloride concentration from lab test results at the research location was determined to be 741 meq/l. According to Appelo & Postma (2005), if the seawater chloride concentration is unknown, it can be assumed to be 566 meq/l, while freshwater chloride can be assumed to be 0 meq/l. The  $f_{sea}$  values at the research location ranged from -0.29% to 1.57%. A negative value indicated that the groundwater at the research location was classified as

fresh water, while a positive value ranging from 0-100% indicated that it was more highly impacted by seawater intrusion. The results of the  $f_{sea}$  calculation are presented in Table 5 and their spatial distribution is shown in Figure 7.

Table 5. Analysis of Seawater Fraction ( $f_{sea}$ ) Results

Geology	Sample ID	TDS	Cl	$f_{sea}$	$f_{sea}(\%)$	Water Type
		ppm	meq/l			
Alluvial	TP 1	367	1.55	-0.001	-0.12	Fresh Groundwater
	TP 2	977	14.00	0.016	1.57	Mixed Groundwater
	TP 3	450	2.80	0.001	0.05	Fresh Groundwater
	TP 4	666	4.20	0.002	0.24	Mixed Groundwater
Volcan (Gabon Formation)	TP 6	149	0.99	-0.002	-0.19	Fresh Groundwater
	TP 7	199	0.95	-0.002	-0.20	Fresh Groundwater
	TP 8	149	0.59	-0.002	-0.25	Fresh Groundwater
Karst (Kalipucang Formation)	TP 9	259	0.35	-0.003	-0.28	Fresh Groundwater
	TP 10	143	0.31	-0.003	-0.29	Fresh Groundwater
Beach Sediment	TP 5	145	0.43	-0.003	-0.27	Fresh Groundwater
	TP 11	96	0.48	-0.003	-0.26	Fresh Groundwater
	Cl seawater		741.00			
	Cl freshwater		2.42			

Tomaszkiewicz et al. (2014) reviewed data from various studies on seawater intrusion worldwide, focusing on the values of  $f_{sea}$ , TDS, and EC. Based on these three parameters, groundwater was categorized into fresh groundwater (average  $f_{sea}$  0.0 to 0.4%; TDS 0-500 mg/l; and EC <700  $\mu\text{S}/\text{cm}$ ), mixed groundwater ( $f_{sea}$  0.1 to 10%; TDS 500-7000 mg/l; and EC 700-10,000  $\mu\text{S}/\text{cm}$ ), saline groundwater (average  $f_{sea}$  16-90%; TDS 7000-15,000 mg/l; and EC 10,000-20,000  $\mu\text{S}/\text{cm}$ ), and seawater ( $f_{sea}$  value of 100%). The  $f_{sea}$  values at the study site ranged from -0.29% to 1.57%, which, according to Tomaszkiwicz et al. (2014), fell into the categories of fresh groundwater and mixed groundwater. Specifically, the  $f_{sea}$  values from -0.29% to 0.05% were classified as fresh groundwater, while the  $f_{sea}$  values of 0.24% and 1.57% fell into the mixed groundwater category, occurring in alluvial geological conditions.

The highest  $f_{sea}$  value, 1.57%, was observed at TP 2. When compared to the  $f_{sea}$  values reported in other studies, this value was relatively low ( $f_{sea}<10\%$ ), as reported by Tomaszkiwicz et al. (2014), Shin et al. (2020), Abu Al Naeem et al. (2019), and Bourjila et al. (2023). For instance, Bourjila et al. (2023) observed an increase in seawater intrusion in the alluvial coast of the Ghis-Nekor Plain over seven years, from 14% to 20%, indicating a progressive increase in seawater intrusion over time. Similarly, in the alluvial coastal region of the Gaza Coastal Aquifer,  $f_{sea}$  values ranged from 11.08% to 48.54%, with approximately 6.4% of all samples showing  $f_{sea}$  values above 20%. The highest value, 48.54%, resulted from paleo seawater transgression Abu Al Naeem et al. (2019). Additionally, Kumar et al. (2020) reported the highest  $f_{sea}$  value of 37.7%, which was attributed to the proximity to salt pans in the coastal aquifer.

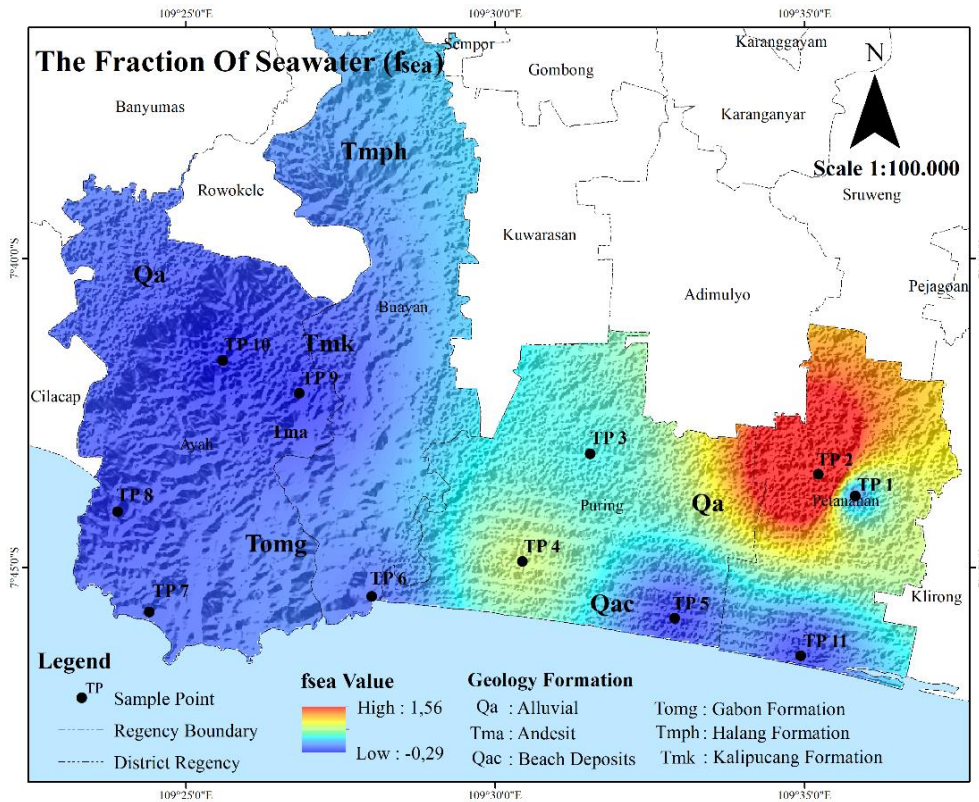


Figure 7. Spatial distribution of the Fraction of Seawater Intrusion ( $f_{sea}$ )

Another  $f_{sea}$  value indicative of mixed groundwater was 0.24% at TP 4, with a TDS value of 666 mg/l. The relatively low  $f_{sea}$  values (0.24% and 1.57%) in areas affected by seawater intrusion, as indicated by the Gibbs diagram analysis, were primarily due to the dominance of water-rock interaction in the hydrochemistry of the groundwater at the study site. This was further characterized by high concentrations of  $Ca^{2+}$  and  $HCO_3^-$ , revealing the water-rock dominance condition (Hasan et al., 2023). According to Shin et al. (2020), the relatively low mixing level between seawater and freshwater was likely influenced by the amount of rainfall in the study area, although in other cases, aquifers intruded by seawater were more affected by tidal fluctuations than by rainfall (Kim et al., 2005).

The distances of TP 2 and TP 4 from the coast were approximately 6.4 km and 2.2 km, respectively. These distances were farther than the intruded areas at Ketah Beach in Situbondo, Borombong in Makassar, and Tegal Coast, which were 1 km, 1.5 km, and 4 km away, respectively (Ismawan et al., 2016; Putri et al., 2016; Yanti et al., 2016). Similar findings were observed in studies by Ouhamdouch et al. (2020) and Behera et al. (2019), which focused on locations near the coast. Therefore, the alluvial coastal area affected by intrusion in this study site was not influenced by tidal fluctuations or high waves but rather by the dominant water-rock interaction in the groundwater at the freshwater-saline water interface. This was also supported by the minimal variation in the results of three ion ratios ( $Mg^{2+}/Ca^{2+}$ ,  $Cl^-/HCO_3^-$ , and  $Mg^{2+}/(Mg^{2+}+Ca^{2+})$ ), indicating geochemical processes such as cation exchange occurring at the study site (Kumar et al., 2020).

The  $f_{sea}$  values characterizing fresh groundwater in the study area ranged from -0.29% to 0.05%, representing approximately 82% of all samples. These  $f_{sea}$  values were predominantly found in volcanic, karst, coastal sediment, and partially alluvial geological conditions. The lowest  $f_{sea}$  values occurred in karst, coastal sediment, and volcanic geological conditions, with a range of -0.29% to -0.19%, indicating no seawater mixing in these areas. Similarly, Kumar et al. (2020) recorded negative  $f_{sea}$  values in a village located far from the coast. Conversely, within the study area characterized by volcanic and coastal sediment geological conditions, which are situated

100-300 meters from the coast, the  $f_{\text{sea}}$  values still indicated fresh groundwater. The karst geological area within the study region is also influenced by the dissolution of carbonate rocks, as characterized by the  $\text{Mg}^{2+}/\text{Ca}^{2+}$  ratio in mmol/l units (Mujib et al., 2024). A  $\text{Mg}^{2+}/\text{Ca}^{2+}$  ratio of  $<0.5$  mmol/l indicates that silicate dissolution also contributes to the dissolution of carbonate rocks, as observed in TP 9 (0.06 mmol/l). In contrast, TP 10 (0.56 mmol/l) suggests that carbonate dissolution is slightly influenced by seawater intrusion.

## CONCLUSION

This study successfully identified and spatially mapped seawater intrusion across different geological conditions in the southern part of Kebumen District using a hydrogeochemical approach. The findings highlight the complex interplay between geological formations and seawater intrusion, with the highest intrusion observed in alluvial and karst regions, particularly at TP 2, TP 4, and TP 10. The use of ion ratios ( $\text{Mg}^{2+}/\text{Ca}^{2+}$ ,  $\text{Cl}^-/\text{HCO}_3^-$ , and  $\text{Mg}^{2+}/(\text{Mg}^{2+}+\text{Ca}^{2+})$ ) and the Fraction of Seawater ( $f_{\text{sea}}$ ) method effectively demonstrates the varying degrees of intrusion, with some areas showing significant seawater influence while others remain largely unaffected. These results underscore the importance of continuous monitoring and the implementation of targeted management strategies to protect vulnerable freshwater aquifers from salinization. Further research was recommended to explore the long-term trends of seawater intrusion in this region and to develop more comprehensive mitigation measures tailored to the unique geological conditions of the study area.

## ACKNOWLEDGMENTS

We thank the Department of Geography Education, Faculty of Education at the University of Jember has facilitated the author's research.

## DECLARATIONS

### Conflict of Interest

We declare no conflict of interest, financial or otherwise.

### Ethical Approval

On behalf of all authors, the corresponding author states that the paper satisfies Ethical Standards conditions, no human participants, or animals are involved in the research.

### Informed Consent

On behalf of all authors, the corresponding author states that no human participants are involved in the research and, therefore, informed consent is not required by them.

## DATA AVAILABILITY

Data used to support the findings of this study are available from the corresponding author upon request.

## REFERENCES

Abu Al Naeem, M. F., Yusoff, I., Ng, T. F., Maity, J. P., Alias, Y., May, R., & Alborsh, H. (2019). A study on the impact of anthropogenic and geogenic factors on groundwater salinization and seawater intrusion in Gaza coastal aquifer, Palestine: An integrated multi-techniques approach. *Journal of African Earth Sciences*, 156, 75–93. <https://doi.org/10.1016/j.jafrearsci.2019.05.006>

Appelo, C. A. J., & Postma, D. (2005). *Geochemistry, groundwater and pollution*. CRC press.

- Ardaneswari, T. A., Yulianto, T., & Putranto, T. T. (2016). Analisis intrusi air laut menggunakan data resistivitas dan geokimia airtanah di dataran aluvial kota Semarang. *Youngster Physics Journal*, 5(4), 335-350.
- Arslan, H. (2014). Estimation of spatial distribution of groundwater level and risky areas of seawater intrusion on the coastal region in Çarşamba Plain, Turkey, using different interpolation methods. *Environmental Monitoring and Assessment*, 186(8), 5123–5134. <https://doi.org/10.1007/s10661-014-3764-z>
- Asikin, S., Handoyo, A., Busono, H., & Gafoer, S. (1992). Geological map of the Kebumen Quadrangle, Jawa (pp. 1401–1).
- Bear, J., Cheng, A., Sorek, S., Ouazar, D., & Herrera, I. (1999). Seawater intrusion in coastal aquifers: concepts, methods, and practices. Retrieved from <https://api.semanticscholar.org/CorpusID:127213695>
- Behera, A. K., Chakrapani, G. J., Kumar, S., & Rai, N. (2019). Identification of seawater intrusion signatures through geochemical evolution of groundwater: a case study based on coastal region of the Mahanadi delta, Bay of Bengal, India. *Natural Hazards*, 97(3), 1209–1230. <https://doi.org/10.1007/s11069-019-03700-6>
- Benaafi, M., Abba, S. I., & Aljundi, I. H. (2023). State-of-the-art on the conceptual advancement of seawater intrusion: A comprehensive review, management, and possible future research direction. *Journal of King Saud University - Science*, 35(6), 102749. <https://doi.org/10.1016/j.jksus.2023.102749>
- Bourjila, A., Dimane, F., Ghalit, M., Taher, M., Kamari, S., El Hammoudani, Y., Achoukhi, I., & Haboubi, K. (2023). Mapping the spatiotemporal evolution of seawater intrusion in the Moroccan coastal aquifer of Ghiss-Nekor using GIS-based modeling. *Water Cycle*, 4, 104–119. <https://doi.org/10.1016/j.watcyc.2023.05.002>
- Cahyadi, A., & Hidayat, W. (2017). Analisis karakteristik hidrogeokimia airtanah Di Pulau Koral Panggal, Kepulauan Seribu, DKI Jakarta. *Jurnal Geografi*, 9, 99–108. <https://doi.org/10.24114/jg.v9i2.6052>
- Cahyadi, A., Marfai, M. A., Tivianton, T., Wulandari, & Hidayat, W. (2017). Kajian distribusi spasial salinitas airtanah berdasarkan kandungan klorida di Pulau Pramuka, Kepulauan Seribu, DKI Jakarta. *Inarxiv (pre-print)*. <https://doi.org/10.31227/osf.io/26bsq>
- Darmanto, D., & Cahyadi, A. (2013). Kajian intrusi air laut melalui sungai di Pesisir Kabupaten Demak Jawa Tengah. *Majalah Geografi Indonesia*, 27(1), 1-10.
- Gemilang, W. A., Wisha, U. J., & Mardyanto, M. A. (2022). Surface groundwater pollution dynamics over 2015-2020 in the salt drying pond of Pademawu Subdistrict, Madura, Indonesia. *Geosfera Indonesia*, 7(1), 1. <https://doi.org/10.19184/geosi.v7i1.28898>
- Hadi, B. S. (2013). Metode interpolasi spasial dalam studi geografi (Ulasan Singkat dan Contoh Aplikasinya). *Geo Media: Majalah Ilmiah Dan Informasi Kegeografian*, 11(2), 235–252.
- Hasan, S. S., Salem, Z. E., & Sefelnasr, A. (2023). Assessment of hydrogeochemical characteristics and seawater intrusion in coastal aquifers by integrating statistical and graphical techniques: quaternary Aquifer, West Nile Delta, Egypt. *Water*, 15(10), 1803. <https://doi.org/10.3390/w15101803>

- Hindarto, T., & Ansori, C. (2021). Pengembangan pariwisata berkelanjutan Grafiti Gua Jatijajar sebagai daya tarik wisata gua. *Jurnal Analisa Sosiologi*, 10(2), 433–451.
- Hussain, M. S., Abd-Elhamid, H. F., Javadi, A. A., & Sherif, M. M. (2019). Management of seawater intrusion in coastal aquifers: a review. *Water*, 11(12). <https://doi.org/10.3390/w11122467>
- Ismawan, Moch. F., Sanjoto, T. B., & Setyaningsih, W. (2016). Kajian Intrusi Air Laut Dan Dampaknya Terhadap Masyarakat Di Pesisir Kota Tegal. *Geo-Image*, 5(1), 1–5.
- Jasechko, S., Perrone, D., Seybold, H., Fan, Y., & Kirchner, J. W. (2020). Groundwater level observations in 250,000 coastal US wells reveal scope of potential seawater intrusion. *Nature Communications*, 11(1), 3229. <https://doi.org/10.1038/s41467-020-17038-2>
- Kazakis, N., Busico, G., Colombani, N., Mastrocicco, M., Pavlou, A., & Voudouris, K. (2019). GALDIT-SUSI a modified method to account for surface water bodies in the assessment of aquifer vulnerability to seawater intrusion. *Journal of Environmental Management*, 235, 257–265. <https://doi.org/10.1016/j.jenvman.2019.01.069>
- Kazakis, N., Pavlou, A., Vargemezis, G., Voudouris, K. S., Soulios, G., Pliakas, F., & Tsokas, G. (2016). Seawater intrusion mapping using electrical resistivity tomography and hydrochemical data. An application in the coastal area of eastern Thermaikos Gulf, Greece. *Science of The Total Environment*, 543, 373–387. <https://doi.org/10.1016/j.scitotenv.2015.11.041>
- Kim, J.-H., Lee, J., Cheong, T.-J., Kim, R.-H., Koh, D.-C., Ryu, J.-S., & Chang, H.-W. (2005). Use of time series analysis for the identification of tidal effect on groundwater in the coastal area of Kimje, Korea. *Journal of Hydrology*, 300(1), 188–198. <https://doi.org/10.1016/j.jhydrol.2004.06.004>
- Kumar, P. J. S., Jegathambal, P., Babu, B., Kokkat, A., & James, E. J. (2020). A hydrogeochemical appraisal and multivariate statistical analysis of seawater intrusion in point calimere wetland, lower Cauvery region, India. *Groundwater for Sustainable Development*, 11, 100392. <https://doi.org/10.1016/j.gsd.2020.100392>
- Kura, N. U., Ramli, M. F., Ibrahim, S., Sulaiman, W. N. A., & Aris, A. Z. (2014). An integrated assessment of seawater intrusion in a small tropical island using geophysical, geochemical, and geostatistical techniques. *Environmental Science and Pollution Research*, 21(11), 7047–7064. <https://doi.org/10.1007/s11356-014-2598-0>
- Manivannan, V., & Elango, L. (2019). Seawater intrusion and submarine groundwater discharge along the Indian coast. *Environmental Science and Pollution Research*, 26(31), 31592–31608. <https://doi.org/10.1007/s11356-019-06103-z>
- Marfai, M. A., & Cahyadi, A. (2017). Karakteristik hidrogeokimia airtanah di Pesisir Kabupaten Demak, Jawa Tengah. *Inarxiv (pre-print)*. <https://doi.org/10.31227/osf.io/grks6>
- Michael, H. A., Post, V. E. A., Wilson, A. M., & Werner, A. D. (2017). Science, society, and the coastal groundwater squeeze. *Water Resources Research*, 53(4), 2610–2617. <https://doi.org/10.1002/2017WR020851>
- Momejian, N., Abou Najm, M., Alameddine, I., & El-Fadel, M. (2019). Groundwater vulnerability modeling to assess seawater intrusion: a methodological comparison with geospatial interpolation. *Water Resources Management*, 33(3), 1039–1052. <https://doi.org/10.1007/s11269-018-2165-4>

- Mujib, M. A., Adji, T. N., Haryono, E., Naufal, M., & Fatchurohman, H. (2024). Karst aquifer characterization by means of its karstification degree and time series analysis (Case: Ngerong Spring in Rengel Karst, East Java, Indonesia). *Indonesian Journal on Geoscience*, 11(1), 45–60. <https://doi.org/10.17014/ijog.11.1.45-60>
- Mujib, M. A., Adji, T. N., Suma, N. N., Ikhsan, F. A., & Indartin, T. R. D. (2020). The quality and usability of spring water for irrigation (case study: Ngerong Spring, Rengel Karst, Tuban, East Java). *IOP Conference Series: Earth and Environmental Science*, 485(1). <https://doi.org/10.1088/1755-1315/485/1/012025>
- Mujib, M. A. (2015). Analisis karakteristik dan tingkat karstifikasi akuifer karst di Sistem Mataair Ngerong, Kecamatan Rengel, Kabupaten Tuban. Thesis. Universitas Gadjah Mada. <http://etd.repository.ugm.ac.id/penelitian/detail/81139>
- Nair, I. S., Brindha, K., & Elango, L. (2021). Assessing the origin and processes controlling groundwater salinization in coastal aquifers through integrated hydrochemical, isotopic and hydrogeochemical modelling techniques. *Hydrological Sciences Journal*, 66(1), 152–164. <https://doi.org/10.1080/02626667.2020.1826490>
- Nair, I. S., Rajaveni, S. P., Schneider, M., & Elango, L. (2013). Identification of seawater intrusion by cl/br ratio and mitigation through managed aquifer recharge in Aquifers North of Chennai, India. *Journal of Groundwater Research*, 2, 155–162.
- Ouhamdouch, S., Bahir, M., & Ouazar, D. (2020). Seawater intrusion into coastal aquifers from semi-arid environments, Case of the alluvial aquifer of Essaouira basin (Morocco). *Carbonates and Evaporites*, 36(1), 5. <https://doi.org/10.1007/s13146-020-00663-9>
- Panjaitan, D., Tarigan, J., Rauf, A., & Nababan, E. S. M. (2018). Determining sea water intrusion in shallow aquifer using Chloride Bicarbonate Ratio Method. *IOP Conference Series: Earth and Environmental Science*, 205(1), 012029. <https://doi.org/10.1088/1755-1315/205/1/012029>
- Papazotos, P., Koumantakis, I., & Vasileiou, E. (2019). Hydrogeochemical assessment and suitability of groundwater in a typical Mediterranean coastal area: A case study of the Marathon basin, NE Attica, Greece. *HydroResearch*, 2. <https://doi.org/10.1016/j.hydres.2019.11.002>
- Parizi, E., Hosseini, S. M., Ataie-Ashtiani, B., & Simmons, C. T. (2019). Vulnerability mapping of coastal aquifers to seawater intrusion: Review, development and application. *Journal of Hydrology*, 570, 555–573. <https://doi.org/10.1016/j.jhydrol.2018.12.021>
- Prusty, P., & Farooq, S. H. (2020). Seawater intrusion in the coastal aquifers of India - A review. *HydroResearch*, 3, 61–74. <https://doi.org/10.1016/j.hydres.2020.06.001>
- Putri, A. W., Suharto, B., & Susanawati, L. D. (2016). Identifikasi pencemaran air tanah akibat intrusi air laut (Studi kasus Pesisir Pantai Ketah Kabupaten Situbondo). *Jurnal Sumberdaya Alam dan Lingkungan*, 2(3), 32-39.
- Radityo, D., Alviyanda, A., Natalia, H. C., Hamdani, A., Huseina, A. A., Denhi, A. D. A., Naufal, R. A., & Zayadah, Z. (2020). Identifikasi Keberadaan Intrusi Air Laut pada Kawasan Pemukiman di Sekitar Pesisir Pantai Daerah Desa Sukajaya Lempasing Kecamatan Teluk Pandan. *Journal of Science and Applicative Technology*, 4(2), 110–115. <https://doi.org/10.35472/jsat.v4i2.366>

- Razi, M. H., Wilopo, W., & Putra, D. P. E. (2024). Hydrogeochemical evolution and water-rock interaction processes in the multilayer volcanic aquifer of Yogyakarta-Sleman Groundwater Basin, Indonesia. *Environmental Earth Sciences*, 83(6). <https://doi.org/10.1007/s12665-024-11477-6>
- Renaldo, A. (2019). Analisis Kualitas Air Pemandian di Desa Ulak Bandung Kecamatan Muara Sahung Kabupaten Kaur Provinsi Bengkulu. Thesis: UIN Raden Intan Lampung.
- Senthilkumar, S., Vinodh, K., Johnson Babu, G., Gowtham, B., & Arulprakasam, V. (2019). Integrated seawater intrusion study of coastal region of Thiruvallur district, Tamil Nadu, South India. *Applied Water Science*, 9(5), 124. <https://doi.org/10.1007/s13201-019-1005-x>
- Setiawan, T. (2014). Proses hidrogeokimia pengontrol salinitas air tanah tidak tertekan di Utara Cekungan Air Tanah Jakarta. *Jurnal Lingkungan Dan Bencana Geologi*, 5(1), 39-51.
- Shin, K., Koh, D. C., Jung, H., & Lee, J. (2020). The hydrogeochemical characteristics of groundwater subjected to seawater intrusion in the Archipelago, Korea. *Water*, 12(6), 1542. <https://doi.org/10.3390/w12061542>
- Singhal, B., & Gupta, R. (2010). *Applied Hydrogeology of Fractured Rocks*. In Applied Hydrogeology of Fractured Rocks by B.B.S. Singhal and R.P. Gupta. Netherlands: Springer., <https://doi.org/10.1007/978-94-015-9208-6>
- Sunardi S.P. (2006). *116 Unsur Kimia Deskripsi dan Pemanfaatannya*. Yrama Widya.
- Thin, P. P., Hendrayana, H., Wilopo, W., & Kawasaki, S. (2018). Assessment of groundwater facies in Wates Coastal Area, Kulon Progo, Yogyakarta, Indonesia. *Journal of Degraded and Mining Lands Management*, 5(4), 1389-1401. <https://doi.org/10.15243/jdmlm.2018.054.1389>
- Tomaszkiewicz, M., Abou Najm, M., & El-Fadel, M. (2014). Development of a groundwater quality index for seawater intrusion in coastal aquifers. *Environmental Modelling & Software*, 57, 13-26. <https://doi.org/10.1016/j.envsoft.2014.03.010>
- Vann, S., Puttiwongrak, A., Suteerasak, T., & Koedsin, W. (2020). Delineation of seawater intrusion using geo-electrical survey in a coastal aquifer of Kamala Beach, Phuket, Thailand. *Water*, 12(2), 506. <https://doi.org/10.3390/w12020506>
- Wang, Z., Wang, S., Liu, W., Su, Q., Tong, H., Xu, X., ... & Liu, J. (2020). Hydrochemical characteristics and irrigation suitability evaluation of groundwater with different degrees of seawater intrusion. *Water*, 12(12), 3460. <https://doi.org/10.3390/w12123460>
- Werner, A. D., Bakker, M., Post, V. E. A., Vandenbohede, A., Lu, C., Ataie-Ashtiani, B., Simmons, C. T., & Barry, D. A. (2013). Seawater intrusion processes, investigation and management: Recent advances and future challenges. *Advances in Water Resources*, 51, 3-26. <https://doi.org/10.1016/j.advwatres.2012.03.004>
- Wilopo, W., Risanti, R., Susatio, R., & Putra, D. P. E. (2021). Seawater intrusion assessment and prediction of sea-freshwater interface in Parangtritis coastal aquifer, South of Yogyakarta Special Province, Indonesia. *Journal of Degraded and Mining Lands Management*, 8(3), 2709-2718. <https://doi.org/10.15243/jdmlm.2021.083.2709>

- Yang, J., Liu, H., Tang, Z., Peeters, L., & Ye, M. (2022). Visualization of Aqueous Geochemical Data Using Python and WQChartPy. *Ground Water*, 60(4), 555–564. <https://doi.org/10.1111/gwat.13185>
- Yanti, H., Yani, A., & Arsyad, M. (2016). Intrusi Air Laut Pantai Barombong Makassar dengan Metode Konduktivitas Listrik. *Jurnal Sains Dan Pendidikan Fisika*, 12(3), 311–315.
- Zamroni, A., Sugarbo, O., Trisnaning, P. T., & Prasetya, H. N. E. (2021). Seawater intrusion prone areas around Yogyakarta International Airport: A geological approach. *IOP Conference Series: Earth and Environmental Science*, 782(2). <https://doi.org/10.1088/1755-1315/782/2/022006>
- Zamroni, A., Sugarbo, O., Trisnaning, P. T., Sagala, S. T., & Putra, A. S. (2021). Geochemical approach for seawater intrusion assessment in the area around Yogyakarta International Airport, Indonesia. *The Iraqi Geological Journal*, 54(1F) 1-11. <https://doi.org/10.46717/igj.54.1F.1ms-2021-06-21>